A&A 457, 581–589 (2006)
DOI: 10.1051/0004-6361:20065005


Astronomy & Astrophysics

# Stellar parameters and evidence of circumstellar activity for a sample of Herbig Ae/Be stars

M. M. Guimarães[1,4], S. H. P. Alencar[1], W. J. B. Corradi[1], and S. L. A. Vieira[2,3]

[1] Departamento de Física - ICEx - UFMG, CP 702, 30123-970 Belo Horizonte, MG, Brazil
e-mail: mmg@ifa.hawaii.edu
[2] Centro Universitário UNA - Campus Estoril/Buritis, Rua José Cláudio Resende 80, 30455-590 Belo Horizonte, MG, Brazil
[3] FEAMIG - Faculdade de Engenharia de Minas Gerais - Unidade Gameleira, Rua Gastão Bráulio dos Santos 837, 30510-120 Belo Horizonte, MG, Brazil
[4] *Present address:* Institute for Astronomy, University of Hawaii, 640 N. Aohoku Place, Hilo, HI 96720, USA

Received 10 February 2006 / Accepted 7 June 2006

**ABSTRACT**

*Aims.* We investigate evidence of accretion in a sample of 15 Herbig Ae/Be stars to determine whether these events originate in a remnant gaseous structure from the primordial cloud (rich in hydrogen) or in a metal-rich body (like comets in our Solar System). During such analysis we also determine precise stellar parameters for this sample of stars.
*Methods.* The stars were observed using high resolution spectroscopy ($R$ = 48 000). A synthetic photospheric spectrum was constructed and then subtracted from the observed one to obtain the circumstellar component. An iterative procedure was applied to find the stellar parameters that were used to build the synthetic photospheric spectrum.
*Results.* Evidence of circumstellar activity were found in four stars: HD 100546, HD 142666, HD 144432 and HD 145718. The presence of redshifted absorption features only in the Balmer lines implies that the accreting material is hydrogen-rich, excluding the possibility that the accretion events might have been created by comet-like bodies. We determined effective temperature, surface gravity, metallicity and the projected rotational velocity for the stars in our sample.

**Key words.** stars: pre-main sequence – stars: activity – techniques: spectroscopic – accretion, accretion disks

## 1. Introduction

Herbig Ae/Be stars (hereafter HAEBE stars) are pre-main sequence, intermediate mass (2 to 10 $M_{\odot}$) stars that show high spectroscopic and photometric variability (e.g. Herbig 1960; Finkenzeller & Mundt 1984; Thé et al. 1994; Vieira et al. 2003). Most of this variability is thought to be due to the interaction of the star with its circumstellar environment, composed of a disc and/or an envelope.

In T Tauri stars accretion and ejection are related to the loss of angular momentum by the system and generally require magnetic fields (i.e. magneto-accretion, Shu et al. 1994; Paatz & Camenzind 1996). Although there has been evidence of accretion and ejection in HAEBE stars (Natta et al. 2000), its correlation with the magnetic field has not been established yet.

Evidence of accretion and ejection can be detected through some characteristic features in the spectrum of the star, such as Redshifted Absorption Components (RACs) and Blueshifted Absorption Components (BACs) (Natta et al. 2000; Mora et al. 2002, 2004). In order to find such circumstellar features it is necessary to remove the photospheric contribution from the observed spectrum, which can be done if one is able to reproduce the stellar photospheric spectrum. However, the high variability level of the HAEBE stars makes it hard to precisely determine the stellar parameters, such as effective temperature ($T_{\rm eff}$), surface gravity ($\log g$), projected rotational velocity ($\upsilon \sin i$) and metallicity ([Fe/H]). Inaccurate stellar parameters lead to poorly constrained synthetic photospheric spectra.

RACs and BACs are often found in several lines in the optical and near infrared spectra of HAEBE stars (Natta et al. 2000; Grinin et al. 2001). In order to better constrain the accretion and ejection episodes, it is important to study the appearance and evolution of these circumstellar absorption components in different lines simultaneously.

We will present the stellar parameters for a sample of 15 HAEBE stars and the evidence of RACs and BACs found in 4 stars. In Sect. 2 we will present the data reduction procedure. In Sect. 3 we describe the method used in the determination of the stellar parameters and the results obtained. In Sect. 4 we present the analysis of the stars that showed evidence of accretion. Some remarks on individual objects are presented in Sect. 5, and the conclusions are outlined in Sect. 6.

## 2. Observational data

Accretion and ejection are clear signatures of a very active circumstellar environment that causes intense spectral and photometric variability. A sample of 15 HAEBE stars that have shown this kind of variability was selected from the catalog published by Vieira et al. (2003) as potential candidates to exhibit observable accretion events. This sample was supplemented by a few stars that have had their circumstellar discs imaged (Augereau et al. 1999, 2001; Grady et al. 1996, 2001).

We obtained high resolution ($\frac{\lambda}{\Delta\lambda}$ = 48 000) échelle spectra, during three nights (7, 8 and 9) in May 2002, with the 1.52 m ESO telescope in La Silla (Chile), coupled to the FEROS échelle spectrograph, covering a wavelength range from 3800 to

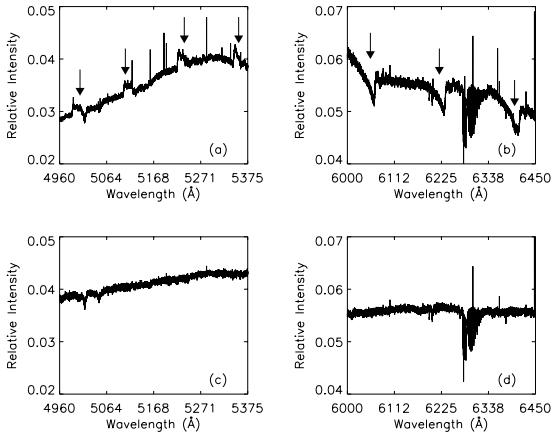


**Fig. 1.** Panels **a)** and **b)** show some artifacts created by a bad reduction of the flat-field image during the automatic procedure. One can see strange spikes (panel **a)**) and absorptions (panel **b)**) in the spectra. Panels **c)** and **d)** show the same region of the spectra of the same star (HD 96042), but now reduced via a manual procedure, where no artifacts can be seen.

8800 Å. The high resolution and the large spectral range allow the observation of small variations in a large number of lines simultaneously. These two features combined can help us to find correlations between the accretion and/or ejection events in all the observed lines.

The data obtained with the FEROS spectrograph are automatically reduced. However, we found some problems with the automatically reduced flat-field images. These reduction problems created artifacts in the stars' spectra, as shown in panels (a) and (b) of Fig. 1.

To solve this problem we used a set of new routines developed by Dr. Herman Hensberge, of the Royal Observatory of Belgium. Examples of the manually reduced spectra are presented in panels (c) and (d) of Fig. 1. The manual reduction of the data followed standard procedures such: flat-field extraction, wavelength calibration with ThAr lamps and cosmic ray extraction. The major problem with the automatic data reduction concerns the choice of the order template. If the star is too bright or too dim, the automatic procedure is not able to find the correct échelle orders because the used template is not the ideal one. The same problem can also be present during the reduction of flat-field and ThAr images. It is solved through the use of new order templates, which can be constructed based on the observed data.

Table 1 presents the observational log for the 15 selected HAEBE stars. Three stars were observed at least 5 times per night (HD 141569, HD 144432 and HD 163296) to search for short timescale spectral variabilities. Four stars presented evidence of circumstellar activity: HD 100546, HD 142666, HD 144432 and HD 145718.

## 3. Stellar parameters

The search for accretion and ejection events in HAEBE stars often requires subtraction of the photospheric contribution from the observed spectrum. This task can be done if we are able to create synthetic spectra based on the stellar parameters. However, the stellar parameters of young stars are very difficult to obtain, due to the high level of activity. In order to obtain such parameters we applied the method described in the following subsections to all stars of our sample.

**Table 1.** Observational data. The columns present the star's identifier (PDS and HD catalogs), right ascension ($\alpha$), declination ($\delta$), number of observed spectra, exposure time (in seconds), magnitude in the $V$ band and the average signal-to-noise ratio, respectively.

| PDS | HD | $\alpha$(2000) | $\delta$(2000) | # | Exp.(s) | $V$ | $S/N$ |
|---|---|---|---|---|---|---|---|
| 303 | 87403 | 10 02 51.5 | –59 16 54.7 | 2 | 900 | 9.24 | 106 |
| 327 | 96042 | 11 03 40.6 | –59 25 59.1 | 3 | 900 | 8.51 | 132 |
| 339 | 100453 | 11 33 05.6 | –54 19 28.5 | 3 | 600 | 7.79 | 108 |
| 340 | 100546 | 11 33 25.4 | –70 11 41.2 | 3 | 500 | 6.70 | 137 |
| 057 | 101412 | 11 39 44.5 | –60 10 27.7 | 3 | 1800 | 9.28 | 98 |
| 069 | Hen 3-949 | 13 57 43.1 | –39 58 45.0 | 3 | 2400 | 9.70 | 65 |
| 395 | 139614 | 15 40 46.4 | –42 29 53.5 | 3 | 900 | 8.25 | 120 |
| 398 | 141569 | 15 49 57.8 | –03 55 16.4 | 14 | 300 | 7.00 | 95 |
| 076 | 142666 | 15 56 40.0 | –22 01 40.0 | 3 | 1200 | 8.81 | 120 |
| 078 | 144432 | 16 06 58.0 | –27 43 09.8 | 15 | 300 | 8.16 | 80 |
| 080 | 145718 | 16 13 11.6 | –22 29 06.6 | 3 | 900 | 8.98 | 110 |
| 473 | 163296 | 17 56 21.3 | –21 57 21.9 | 20 | 300 | 6.87 | 116 |
| 514 | 169142 | 18 24 29.8 | –29 46 49.4 | 3 | 600 | 8.15 | 121 |
| 545 | 174571 | 18 50 47.2 | 08 42 10.1 | 3 | 1500 | 8.89 | 118 |
| 564 | 179218 | 19 11 11.3 | 15 47 15.6 | 3 | 400 | 7.20 | 113 |

### 3.1. Outline of the method

The method used to find the stellar parameters of each star is similar to the one described by Merin et al. (2004) and is based on the following steps:

1. construction of synthetic photospheric spectra for the Balmer lines, using an initial input for the values of $T_{\rm eff}$, $\upsilon \sin i$ and [Fe/H] and several values of $\log g$;
2. measurement of the Balmer line profiles width at an intensity level of 0.8 of the continuum ($I = 0.8$);
3. use of this width as the independent variable in a linear fit procedure to find the best value for $\log g$;
4. use of the best value of $\log g$, found in the previous step, to find the best values of $T_{\rm eff}$, $\upsilon \sin i$ and [Fe/H] that fit the metallic lines of each star. The metallic lines were chosen among those that remained constant during all the observations and are called "pure photospheric lines";
5. use these new values of $T_{\rm eff}$, $\upsilon \sin i$ and [Fe/H] as input to find the $\log g$ again until convergence is achieved.

The Balmer lines are selected to find $\log g$ because their wings are very sensitive to changes in the star's surface gravity, while the metallic lines are used because they are extremely sensitive to changes in the star's temperature and metallicity. The measurement of the width of the Balmer line profiles at an intensity of 0.8 of the continuum avoids small subtleties due to the normalization procedure.

### 3.2. Fit of parameters

To fit the stellar parameters we divided our sample into three groups.

Group 1: $T_{\rm eff} < 8000$ K; where the relationship between the Balmer line width and $\log g$ is not linear;
Group 2: $9000 < T_{\rm eff} < 15\,000$ K; where the photospheric lines are clearly visible and there is a linear relationship between the Balmer line width and $\log g$;
Group 3: $T_{\rm eff} > 15\,000$ K; where the almost complete absence of photospheric lines prevents us from applying the proposed method.

We have made use of the SME code, by Valenti & Piskunov (1996), to build the grids of synthetic spectra. This code also allows us to vary the following parameters: $T_{\rm eff}$, $\log g$, $\upsilon \sin i$,

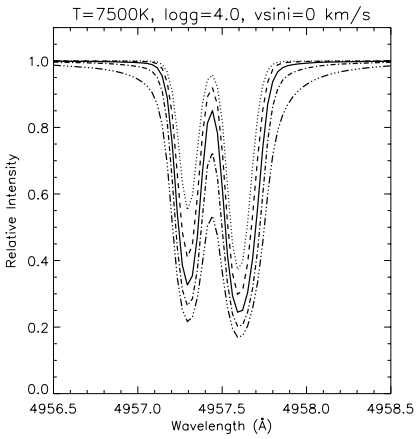


**Fig. 2.** Example of the [Fe/H] influence on the Fe I 4957 photospheric line profile. All profiles were generated with the following physical parameters: $T_{\rm eff} = 7500$ K, $\log g = 4.0$ and $\upsilon \sin i = 0$ km s$^{-1}$. Solid line [Fe/H] = 0.0, dotted line [Fe/H] = –1.0, dashed line [Fe/H] = –0.5, dashed-dotted line [Fe/H] = +0.5 and dashed-dotted-dotted line [Fe/H] = +1.0. As one can see the profile gets deeper as the metallicity increases.

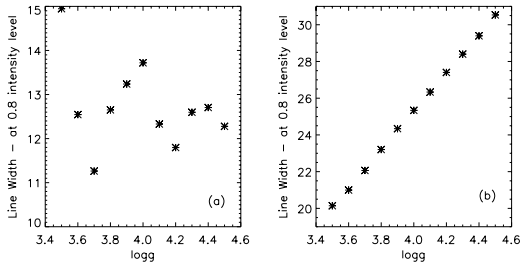


**Fig. 3.** Behavior of $\log g$ for Groups 1 and 2. Panel **a)** shows the H$\gamma$ line width *versus* $\log g$ for a star (HD 142666) of Group 1 ($T_{\rm eff} < 8000$ K) and panel **b)** for a star (HD 100546) of Group 2 ($9000 < T_{\rm eff} < 15\,000$ K). In the second case the linear correlation is clear, whereas there is no correlation in the first case.

[Fe/H], micro and macro turbulent velocities and radial velocity. Following Dunkin et al. (1997), parameters such as micro and macro turbulent velocities were kept constant at 2 and 5 km s$^{-1}$, respectively. As a starting point we used the $T_{\rm eff}$ values determined by Vieira et al. (2003) and solar metallicity ([Fe/H] = 0.0). The radial velocity can be estimated by the code and its value was left free during the fit. The $\upsilon \sin i$ value was found by leaving it as a free parameter at the beginning of the calculations. The convergence is very fast and only minor changes (less than 1 km s$^{-1}$) are necessary at the end of the calculations. The metallicity of the star, represented by the [Fe/H] parameter, is very important because it can change the values of $T_{\rm eff}$ and $\log g$. Figure 2 shows the influence of different values of [Fe/H] in a synthetic photospheric spectrum of fixed $T_{\rm eff}$ and $\log g$. Based on such variability we decided to leave [Fe/H] as a free parameter during the fit.

There is a difference in the method used to fit $\log g$ for the Group 1, because the variation of the width of the Balmer lines, in this case, is not linear with the $\log g$ value, as can be seen in Fig. 3. Therefore we selected the values of $\log g$ that produced synthetic spectra whose width, measured at an intensity level of 0.8, differed by no more than 1% from the width of the observed Balmer lines at the same intensity level. This procedure yields many $\log g$ values for a single line width. The only way to find the best value, and its error, is to build a grid of synthetic spectra for each $\log g$ value, varying the values of $T_{\rm eff}$, $\upsilon \sin i$ and [Fe/H]. For Group 1 stars the error of each parameter is larger than for Group 2 stars, due to uncertainties in the $\log g$ determination.

### 3.3. Error determination and results

The determination of precise parameters for young stars is a difficult task because the line profile can change over short periods. As an example, some of the lines of HD 141569 are so variable (e.g. Mg II 4481 Å) that it is hard to find stable lines to determine the photospheric parameters. In some cases the high $\upsilon \sin i$ merges the lines, making it much more difficult to obtain precise fit parameters.

Pre-main sequence stars show large photometric variations that may lead to wrong parameters if one relies only on photometric data. To overcome these problems we used high S/N spectra with large wavelength range and we have chosen only lines that were stable during our observations and those that were symmetric. By symmetric we mean lines that do not show clear evidence of RACs and BACs.

For each group of stars there is a different way to determine the error of the parameters. Since $\log g$ for Group 2 is well determined, the error calculation follows the steps below:

- a grid of synthetic photospheric spectra is constructed, keeping $\log g$ constant and varying $T_{\rm eff}$ and [Fe/H]. Different sets of solutions are created by different pairs of $T_{\rm eff}$ and [Fe/H];
- a solution ($T_{\rm eff}$, $\log g$ and [Fe/H]) is acceptable if it is not different by more than 1% from the observed spectrum;
- some sets of solutions are discarded based on the presence or absence of helium and metallic lines;
- the error for each parameter represents its possible value within the accepted set of solutions.

To obtain the errors for Group 1 stars it is necessary to check for degenerate solutions, as follows:

- for each possible value of $\log g$ we construct a grid of synthetic spectra, varying $T_{\rm eff}$ and [Fe/H];
- we select the sets of parameters ($\log g$, $T_{\rm eff}$, [Fe/H]) that fit the observed spectra;
- based on some criteria (e.g. presence and fit of metallic lines) we exclude some sets of values. As an example, for an F0 star that presents several metallic lines, pairs of $T_{\rm eff}$ and $\log g$ such as $T_{\rm eff} = 12\,000$ K and $\log g = 5.0$, or $T_{\rm eff} = 4000$ K and $\log g = 3.0$ do not represent good solutions and are discarded;
- the acceptable sets of values are used as the final values and errors.

For Groups 1 and 2, we searched for solutions varying the following parameters within the respective intervals, $\log g \pm 1.0$ dex, $\upsilon \sin i \pm 5$ km s$^{-1}$ and [Fe/H] $\pm 2.0$ dex. The only difference is the temperature interval, for Group 1 we used $T_{\rm eff} \pm 1000$ K while for Group 2 we used $T_{\rm eff} \pm 2000$ K. The maximum and minimum values used during this procedure do not correspond to the errors themselves, they just define an interval within which we searched for degenerate solutions.

The parameters obtained for each star are listed in Table 2. Some values agree very well with the most recently published values, although a few discrepancies exist for some objects, such as HD 169142, presented in Sect. 5.

**Table 2.** Stellar parameters. The columns present the star's identifiers, $T_{\rm eff}$ and error, $\upsilon \sin i$ and error, $\log g$ and error and the metalicity [Fe/H] and error.

| PDS | HD | $T_{\rm eff}$ (K) | $\Delta T_{\rm eff}$ | $\upsilon \sin i$ (km s$^{-1}$) | $\Delta\upsilon \sin i$ | $\log g$ | $\Delta \log g$ | [Fe/H] | $\Delta$[Fe/H] |
|---|---|---|---|---|---|---|---|---|---|
| 303 | 87403 | 10000 | 500 | 105 | 5 | 3.3 | 0.1 | 0.0 | 0.3 |
| 339 | 100453 | 7400 | 400 | 48 | 2 | 4.2 | 0.1 | 0.3 | 0.3 |
| 340 | 100546 | 10000 | 1000 | 60 | 5 | 4.2 | 0.2 | –1.4 | 0.2 |
| 057 | 101412 | 10000 | 1000 | 7 | 1 | 4.1 | 0.4 | –1.0 | 0.2 |
| 395 | 139614 | 7400 | 200 | 25 | 1 | 4.0 | 0.4 | –0.5 | 0.1 |
| 398 | 141569 | 10000 | 200 | 230 | 10 | 4.3 | 0.1 | –0.4 | 0.1 |
| 076 | 142666 | 7500 | 500 | 66 | 3 | 4.3 | 0.1 | 0.2 | 0.2 |
| 078 | 144432 | 7300 | 300 | 80 | 5 | 3.4 | 0.2 | 0.3 | 0.2 |
| 080 | 145718 | 7500 | 200 | 115 | 5 | 3.4 | 0.1 | 0.0 | 0.1 |
| 473 | 163296 | 9400 | 200 | 130 | 10 | 4.1 | 0.1 | 0.5 | 0.1 |
| 514 | 169142 | 7500 | 200 | 55 | 5 | 3.7 | 0.1 | –0.5 | 0.1 |
| 564 | 179218 | 9500 | 500 | 72 | 3 | 4.0 | 0.1 | –0.5 | 0.1 |

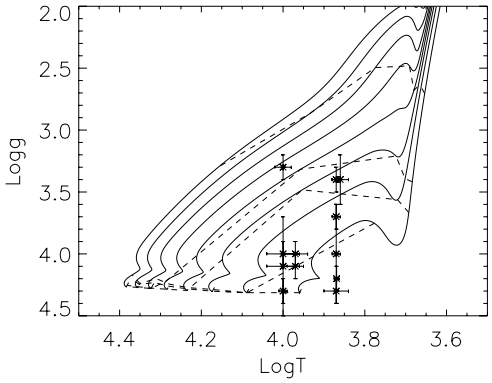


**Fig. 4.** Evolutionary tracks from 2 up to 7 $M_{\odot}$ with steps of 1 $M_{\odot}$. The isochrones are plotted with dashed lines, starting at 0.25 Myr, at the top of the HR diagram, until 10 Myr, bottom of the tracks. The stars are plotted with the respectives error bars.

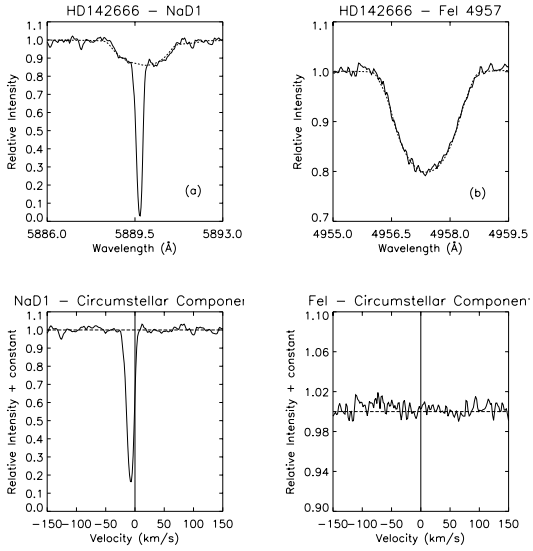


**Fig. 5.** Example of metallic lines that do not present RACs. In the top panels the dashed line represents the synthetic model and the solid line represents the observed spectrum, while in the bottom panels the solid line represents the circumstellar component and the dashed line represents the intensity level at 1.0. Panel **a)** shows the Na I D1 (5889.95 Å) where it is possible to see the narrow interstellar component. We notice that the synthetic spectrum is a very good fit to the photospheric one. The circumstellar component is showed in the lower panel. Panel **b)** presents the Fe I (4957 Å) where we see that the synthetic spectrum fits the photospheric one very well. In the lower panel we can see the circumstellar component where no RAC was detected.

In order to check the evolutionary status of the HAEBE stars we used the $T_{\rm eff}$ and $\log g$ values to plot these stars in an HR diagram, together with a set of PMS evolutionary tracks, as shown in Fig. 4. The evolutionary tracks were computed using the `ATON 2.0` stellar evolution code (Mazzitelli 1989; Mazzitelli et al. 1995; Ventura et al. 1998). Details can be seen in Vieira et al. (2003).

We can divide our sample in three groups in the HR diagram of Fig. 4. The first group contains very young stars with ages below 1.0 Myr (HD 87403, HD 144432 and HD 145718). The second group is composed of stars with ages between 1.0 and 5.0 Myr (HD 101412, HD 163296, HD 169142 and HD 179218). And the third group with more evolved stars with ages above 5.0 Myr (HD 100453, HD 100546, HD 139614, HD 141569, HD 142666). We have not found any correlation between age and circumstellar activity since the stars that presented evidence of accretion have ages spread between 0.5 and 10 Myr.

## 4. Accretion episodes

To quantify the absorption produced by the circumstellar environment we followed the definitions made by Natta et al. (2000). The depth of the circumstellar absorption component ($\tau$) is defined as:

$$\tau = 1 - \frac{F_{\rm obs}}{F_{\rm syn}} \qquad (1)$$

where $F_{\rm obs}$ and $F_{\rm syn}$ represent respectively the observed and the synthetic photospheric intensity at peak wavelength. The above definition shows us that when $\tau = 1$ the circumstellar line is saturated and when $\tau = 0$ there is no circumstellar contribution.

As suggested by Natta et al. (2000), the RACs may originate in a gaseous structure falling from the disc (or envelope) towards the star or in a comet-like body in a star-grazing orbit. In the first case we expect to see RACs in the Balmer lines and in some metallic lines such as Na I D and Ca II. On the other hand, we expect to see RACs with a much larger optical depth in metallic lines than in the Balmer lines when a comet-like body evaporates in its star-grazing orbit towards the star, because such solid bodies should be highly hydrogen depleted. However, while we often see RACs in the Balmer lines of our stars, we do not observe any RAC in metallic lines in our sample. This can be seen in Fig. 5, where we show the observed (solid lines) and synthetic (dashed lines) spectra of the Na I D1 and Fe I (4957 Å) regions

obtained in our last observing night (JD = 2 452 404). These lines were observed simultaneously with the Balmer lines shown in Fig. 7. We see that at JD = 2 452 404 we have the presence of a strong redshifted absorption component in all the Balmer lines, while no RACs are seen in the metallic lines of Fig. 5.

It is possible to study the dynamics of the accretion if one is able to obtain several spectra in which there is evidence of accretion (RACs). The behavior of the velocity of the RACs suggests whether the gas is falling towards the star driven or not by magnetic field lines. If the star is photometrically variable it is necessary to flux calibrate the spectra so one can determine if the variation of the line depth is due to a variation in the star's total flux. We do not have simultaneous photometry so we cannot calibrate the spectra, however based on the variation of the RACs' radial velocity it is possible to determine the dynamics of the material falling towards the star.

Four out of twelve stars with stellar parameters listed in Table 2 are photometrically stable according to the present literature (HD 87403, HD 100453, HD 144432 and HD 169142), five are photometrically variable (HD 100546, HD 141569, HD 142666, HD 145718 and HD 163296) and three do not present enough information in the literature to confirm any photometric behaviour.

The next subsections will show our analysis for three HAEBE stars that showed evidence of accretion.

### 4.1. HD 142666

This star, catalogued as A8V by SIMBAD, is located at the star forming region Sco R1 (following Vieira et al. 2003) at a distance of 100–160 pc, according to Racine (1968). The stellar parameters found in the literature range from an A5V ($T_{\rm eff} = 8250$ K and $\log g = 4.5$, Malfait et al. 1998; Meeus et al. 1998) to A8Ve ($T_{\rm eff} = 7150$ K and $\log g = 4.4$, Dunkin et al. 1997).

The parameters found by Meeus et al. (1998) were based on photometric observations in the optical and ultraviolet regions together with the fit of atmosphere models while Dunkin et al. (1997) have made a spectral classification using échelle spectra. Figure 6 shows the comparison between the stellar parameters found by us and those found in the literature. As can be seen the values from Dunkin et al. (1997) are in good agreement with ours, but disagree with the results by Meeus et al. (1998) and the SIMBAD database.

HD 142666 is photometrically variable comparing data in the literature (Slawson et al. 1992; Malfait et al. 1998; Oudmaijer et al. 2001; Vieira et al. 2003). The amplitude of variation can reach up to ∼1.0 in $V$ on a time scale of months (Meeus et al. 1998). Kurtz & Müller (2001) also reported that this star presents $\delta$ Scuti pulsations with a period of 61 minutes and an amplitude of 0.01 mag in the $B$ filter. Since we do not have simultaneous photometry, it is not possible to determine whether the changes in the absorption depths are due to changes in the star's total flux. We will restrict our analisys to the changes in the RACs' radial velocity.

We have found RACs only in the Balmer lines such as H$\beta$, H$\gamma$ and H$\delta$, as shown in Fig. 7, where the top panels show the observed and synthetic spectrum for each line and the bottom ones present the respective circumstellar components. The RACs are marked, in the bottom panels, by dashed vertical lines. The velocities of the RACs and BACs are listed in Table 3.

H$\beta$ and H$\gamma$ lines exhibited clear evidence of RACs in all the nights observed. The H$\delta$ line also presented evidence of accretion but the absorption feature found in the first night is more complex than the features observed on the other nights. From Table 3 one may see that the RACs' velocity increases with time. Such behavior might be explained by the assumption that the gaseous structure is falling towards the star. The velocity was taken as the center of a Gaussian curve that fits the circumstellar feature. The material falling towards the stars seems to be rich in hydrogen, since RACs were observed only in the Balmer lines.

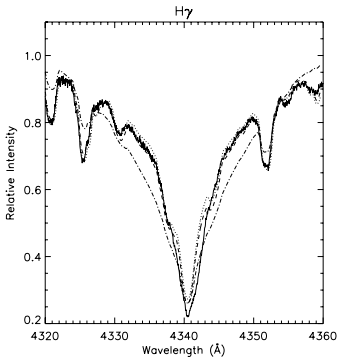


**Fig. 6.** Comparison between our results and the results from the literature for HD 142666. The synthetic spectrum obtained with the parameters we determined is shown as a dashed line, the one calculated with Dunkin et al. (1997) values correspond to the dotted line and the stellar parameters obtained by Meeus et al. (1998) yield the synthetic spectrum shown as a dot-dashed line.

**Table 3.** Velocities of the RACs and BACs found in HD 142666.

| Date | H$\beta$ $V$ (km s$^{-1}$) | H$\gamma$ $V$ (km s$^{-1}$) | H$\delta$ $V$ (km s$^{-1}$) |
|---|---|---|---|
| 07 May 2002 | 132 | 104 | 30 |
| | –30 | –30 | |
| 08 May 2002 | 134 | 116 | 101 |
| | –95 | –72 | –77 |
| 09 May 2002 | 143 | 140 | 133 |
| | 7 | | |

The BACs observed in HD 142666 showed some similarities in H$\beta$ and H$\gamma$ lines. Once more, the complex feature observed in the first night in the H$\delta$ line prevents us from performing a better analysis. From the values of Table 3 we see that the BACs' velocities increase, in modulus, from the first to the second night.

### 4.2. HD 145718

This star, also known as V718 Sco, is catalogued as an A8III/IV by SIMBAD, its distance is 130 ± 20 pc (Perryman et al. 1997) and it is likely associated with the $\rho$ Oph cloud (110–160 pc, e.g. Franco 1990). It was classified by Koch et al. (1963) as an eclipsing binary of Algol type but following Friedemann et al. (1996) and van der Veen et al. (1994) its classification as a binary is still uncertain and more observations are required. HD 145718 is photometrically variable, presenting a small magnitude variation (∼1% in $V$) comparing data in the literature (Wolf & Kern 1983; Slawson et al. 1992; Vieira et al. 2003). We will therefore assume that the photometric variability will not affect our analysis of the RACs optical depth.

We have found evidence of accretion in the Balmer lines, mainly H$\beta$, H$\gamma$ and H$\delta$, as shown in Fig. 8. The velocities of the RACs, obtained in the same manner as for HD 142666, are listed in Table 4, together with the circumstellar absorption depth ($\tau$).

In all lines, both the velocity and $\tau$ decrease with time. This behavior is not straightforwardly explained in a scenario where

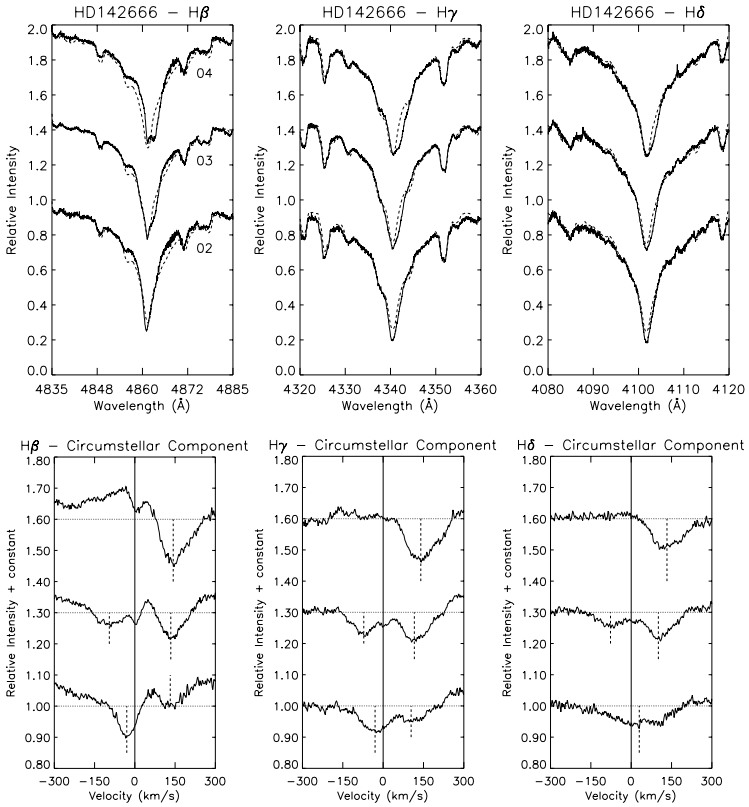


**Fig. 7.** Evidence of accretion and ejection of matter found in the circumstellar component of the Balmer lines of HD 142666. The solid curves represent the observed spectra while the dashed curves represent the synthetic line profile. The *top panels* show the observed and synthetic Balmer lines, from left to right we have H$\beta$, H$\gamma$ and H$\delta$. The *bottom panels* show the circumstellar components of the Balmer lines. In the circumstellar component we also plot a straight line to mark the star's zero velocity reference, dashed lines to mark the RACs and BACs and a dotted line to show the zero absorption level. In each panel the spectra are ordered from bottom to top according to the date of observation (JD-2 452 400), as shown in the H$\beta$ panel.

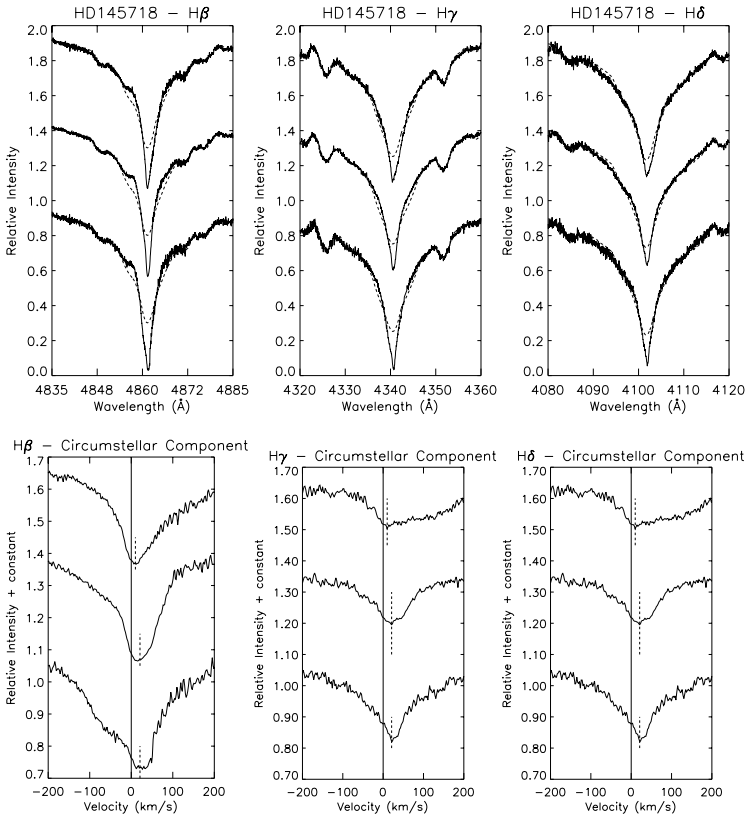


**Fig. 8.** Same caption as Fig. 7 but for the HAEBE star HD 145718.

**Table 4.** Velocities and $\tau$ values of the RACs found in HD 145718.

| Date | H$\beta$ | | H$\gamma$ | | H$\delta$ | |
|---|---|---|---|---|---|---|
| | $V$ (km s$^{-1}$) | $\tau$ | $V$ (km s$^{-1}$) | $\tau$ | $V$ (km s$^{-1}$) | $\tau$ |
| 07 May 2002 | 27 | 0.90 | 27 | 0.86 | 21 | 0.76 |
| 08 May 2002 | 16 | 0.77 | 16 | 0.60 | 21 | 0.45 |
| 09 May 2002 | 12 | 0.77 | 4 | 0.59 | 10 | 0.42 |

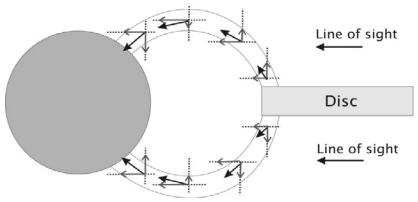


**Fig. 9.** Example of magnetoaccretion where we see the tubes leaving the disc surface and reaching the star. The trajectory followed by the gas toward the star is represented by the arrows. The decomposition of the velocity vector in the line of sight shows that such accretion model qualitatively explains the observed behavior of the RACs.

the RACs originate from accreting material that falls towards the star. However, such behavior might be explained assuming that the gaseous structure is falling into the star driven by dipolar magnetic field lines. The RAC's velocity is the projected velocity in our line of sight and as such it decreases near the star for the case of a line of sight parallel to the disc (near edge-on system), as shown in Fig. 9.

Following Shu et al. (1994) we calculated the truncation radius of the inner disc ($R_t$), from where the material falls into the star via magnetic field lines. The star's radius ($R_\star = 5.7\ R_\odot$) was calculated based on our $\log g$ value and the mass ($M_\star \sim 3\ M_\odot$) was determined using the ATON 2.0 stellar evolution code. We used a magnetic field strength of $B_\star = 1$ kG, even knowing that there are no observational measurements of such a strong magnetic field in HAEBE stars. Young early-type stars are not expected to have magnetic fields due to a dynamo type of activity as strong as those measured in T Tauri stars, but some main sequence A stars actually do show magnetic fields of the order of kG (Borra et al. 1982). Only recently was the longitudinal magnetic field measured at a level higher than $3\sigma$ by Hubrig et al. (2006) and Wade et al. (2005), obtaining fields of the order of $10^2$ G. We also noted that values of $B_\star$ ranging from 100 G to 10 kG do not change significantly the value of the infall velocity.

Muzerolle et al. (2004), however, have successfully fitted magnetospheric accretion models to the Balmer and NaD emission lines of UX Ori (an A2 star), suggesting that magnetospheric accretion could be important in intermediate mass objects. Muzerolle et al. (2004) also showed that models of the accretion shock can explain the observed excess flux in the Balmer discontinuity for a large number of HAEBE stars, implying mass accretion rates smaller than $\sim 10^{-7}\ M_\odot\,\mathrm{yr}^{-1}$. We then adopted $\dot{M} \sim 10^{-8}\ M_\odot\,\mathrm{yr}^{-1}$, as a reasonable value for a HAEBE star. With the above parameters we obtained a truncation radius of $R_t \sim 13\ R_\odot$. Assuming that the material starts its fall from rest and free falls onto the star via magnetic field lines we evaluate its final velocity as $\sim$430 km s$^{-1}$. The geometry of the accretion process, indicated by Fig. 9, together with the supposed line of sight, shows that during the fall there is a point where the projected velocity equals the infall velocity, and after that the projected velocity always decreases. From this point to the stellar surface, we estimated an infall time of about half a day. Thus, qualitatively, the magneto-accretion model could explain the behavior of the RACs for this star. However, quantitatively, the model shows that the time necessary for infall is much less than the observed time. Estimates of individual mass accretion rates and of the magnetic field strength are, however, needed for a more accurate evaluation of the importance of magnetospheric accretion to HAEBE stars.

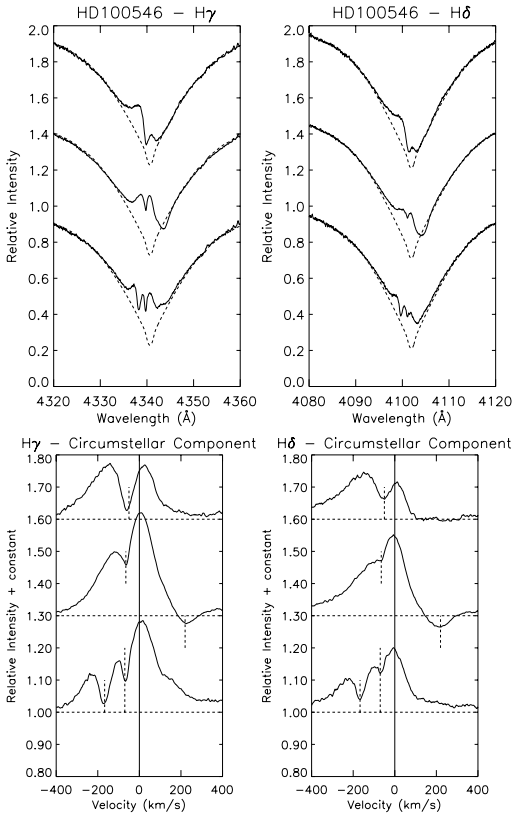


**Fig. 10.** Same caption as Fig. 7 but for the HAEBE star HD 100546.

### 4.3. HD 100546

This Herbig Be star is classified as B9.5Ve, at a distance of 103 ± 6 pc, with an estimated age ~10 Myr, following van den Ancker et al. (1997). Our results, mainly the $\log g$ value, indicate an age between 5 and 10 Myr. The determination of $\log g$ for this star is shown in panel b of Fig. 3. A circumstellar disc was revealed by visible and infrared imaging (Grady et al. 2001; Augereau et al. 2001) and evidence of accretion were reported by Vieira et al. (1999). Our results indicate that this star is deficient in Fe which corroborates the results from Acke & Waelkens (2004). This star is photometrically constant within ~1% in $V$, by comparing data in the literature (Hu et al. 1989; Slawson et al. 1992; Malfait et al. 1998; de Winter et al. 2001; Vieira et al. 2003). We will therefore assume that the photometric variability will not affect our analysis of the RACs optical depth.

Figure 10 shows the spectra and circumstellar components for H$\gamma$ and H$\delta$ Balmer lines. Evidences of ejection are clearly visible in the blue circumstellar component, for all the nights. The second night also shows evidence of accretion in both lines. The velocity and $\tau$ values are presented in Table 5.

The RACs and BACs present in our observations of HD 100546 do not show any systematic behavior, so it is not possible to establish any coherent formation scenario for such structures based only on our 3 spectra. Higher temporal resolution is necessary in this case.

**Table 5.** Velocities and $\tau$ values of the RACs and BACs found in HD 100546.

| Date | Hγ | | Hδ | |
|---|---|---|---|---|
| | $V$ (km s$^{-1}$) | $\tau$ | $V$ (km s$^{-1}$) | $\tau$ |
| 07 May 2002 | –172 | –0.07 | –167 | –0.11 |
| | –66 | –0.30 | –70 | –0.44 |
| 08 May 2002 | 225 | 0.06 | 220 | 0.09 |
| | –63 | –0.50 | –65 | –0.65 |
| 09 May 2002 | –63 | –0.08 | –50 | –0.25 |

## 5. Remarks on individual stars

**HD 101412:** This star has the lowest $\upsilon \sin i$ value of all the sample (see Table 2), which suggests that we see it almost pole on. It is classified as B9.5 V in the SIMBAD database but we estimate it to be an A0 III/IV star, based on our temperature and surface gravity values.

**HD 139614:** The parameters we have found for this star do not agree with the parameters from Dunkin et al. (1997) ($T_{\rm eff} = 8250$ K, $\log g = 4.2$, $\upsilon \sin i = 24$ km s$^{-1}$, [Fe/H] = –0.16) and Acke & Waelkens (2004) ($T_{\rm eff} = 8000$ K, $\log g = 4.5$, $\upsilon \sin i = 24$ km s$^{-1}$, [Fe/H] = –0.3). Their temperature does not fit the observed lines, in a similar way to HD 169142 as shown in Fig. 11.

**HD 144432:** An extensive discussion about this star was provided by Pérez et al. (2004); it is classified as A9/F0V while our results show a discrepancy in the luminosity class, given its $\log g$. Pérez et al. (2004) also found a probable companion, of K type, for this star, through optical and near-IR imaging. We also corroborate the Li I 6707.8 Å detection in the HD 144432 spectra, observed by Pérez et al. (2004), which adds support to the pre-main sequence nature of this star. We have found BACs in the Balmer lines together with large variations in other lines, such as Mg II 4481 Å, He I 5876 Å and Na I D1. We will use our 15 spectra, collected in this mission, to perform a detailed analysis together with the correlation between the variable lines and a model able to explain such variations. Such work will be presented in a future paper.

**HD 169142**: This star has a spectral type B9Ve listed in the SIMBAD database, A5Ve by Dunkin et al. (1997) (spectral classification with échelle spectra) and a spectral type A9III/IVe from our fit and from Vieira et al. (2003). As an example we show the parameters we have found for this object together with the values found in the literature in Fig. 11. It can be seen that the values taken from SIMBAD and from Dunkin et al. (1997) do not fit the observed lines. The absence of He I lines indicates that this star does not have a spectral type B9V as also noted by Dunkin et al. (1997).

## 6. Conclusions

The method described in this work has enabled us to obtain the stellar parameters, $T_{\rm eff}$, $\log g$, $\upsilon \sin i$ and [Fe/H], for a sample of 15 HAEBE stars. For some objects it was the first time that such parameters were obtained. Synthetic photospheric spectra were constructed and subtracted from the observed ones in order to obtain the circumstellar component, where we have looked for evidence of accretion. Three stars exhibited evidence of accretion, HD 100546, HD 142666 and HD 145718 and the behavior of the RACs was different in each case.

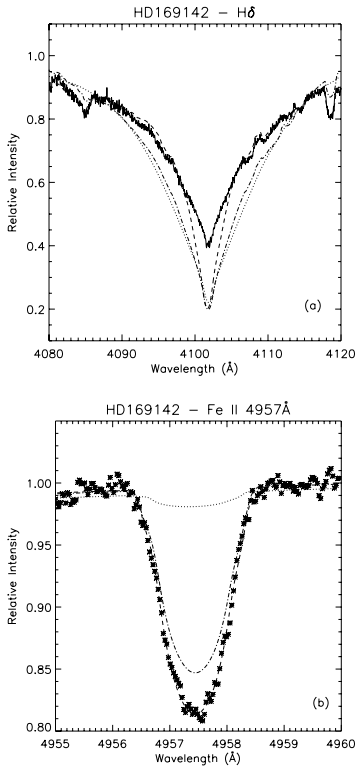


**Fig. 11.** Comparison between our results and the results from literature for HD 169142. The solid curve represents the observed spectrum, the dashed line represents the synthetic spectrum built with our parameters while the dot-dashed and dotted lines represent the synthetic spectra built with the parameters of Dunkin et al. (1997) and SIMBAD, respectively. Panel **a)** shows the Hδ line profile and panel **b)** shows the Fe II 4957 Å line.

The RACs observed in HD 142666 exhibited a behavior expected from an infalling gaseous structure, rich in hydrogen, that was problably part of the inner disc of the star. There is also evidence for BACs in the circumstellar components of the first and second nights, but not in the third night. The kinematic behavior is similar to the one of RACs.

The velocity behavior of the HD 145718's RACs is oposite to the one exhibited by HD 142666. The velocity of the absorption feature diminishes along the observations. This behavior might be qualitatively explained by the assumption of magnetospheric accretion. However, more spectra and more detailed modelling work are needed for a quantitative explanation.

The RACs oberved in HD 100546 do not show any systematic behavior. More observations with a higher temporal coverage are necessary to better understand the accretion and ejection events.

Despite the different kinematic behavior of the RACs, their presence in the Balmer lines show that the accreting material in these HAEBE stars is rich in hydrogen, what discards the possibility of an origin in comet-like bodies in star-grazing orbits. However, to better understand the dynamics of the accretion process in HAEBE stars a systematic observational campaign is necessary.

*Acknowledgements.* M.M.G. acknowledges support from Laboratório Nacional de Astrofísica, CAPES (PROF program), CNPq. We also thank Dr. Herman Hensberge for help with the reduction of FEROS data and Dr. Luiz T. S. Mendes for the evolutionary tracks. SHPA acknowledges support from CAPES (PRODOC program) and CNPq (201228/2004-1). WJBC acknowledges support from FAPEMIG (EDT-1883/03 and CEX-961/04).

## References


Acke, B., & Waelkens, C. 2004, A&A, 427, 1009
Augereau, J. C., Lagrange, A. M., Mouillet, D., & Menard, F. 1999, A&A, 350, 51
Augereau, J. C., Lagrange, A. M., Mouillet, D., & Menard, F. 2001, A&A, 365, 78
Borra, E. F., Landstreet, J. D., & Mestel, L. 1982, ARA&A, 20, 191
Dunkin, S. K., Barlow, M. J., & Ryan, S. G. 1997, MNRAS, 286, 604
de Winter, D., van den Ancker, M. E., Maira, A., et al. 2001, A&A, 380, 609
Finkenzeller, U., & Mundt, R. 1984, A&AS, 55, 109
Franco, G. A. P. 1990, A&A, 227, 499
Friedemann, C., Gürtler, J., & Löwe, M. 1996, A&AS, 117, 205
Grady, C. A., Pérez, M. R., Talavera, A., et al. 1996, A&AS, 120, 157
Grady, C. A., Polomski, E. F., Henning, Th., et al. 2001, AJ, 122, 3396
Grinin, V. P., Kozlova, O. V., & Natta, A., et al. 2001, A&A, 379, 482
Herbig, G. H. 1960, ApJS, 4, 337
Hubrig, S., Yudin, R. V., Schöller, M., & Pogodin, M. A. 2006, A&A, 446, 1089
Hu, J. Y., Thé, P. S., & de Winter, D. 1989, A&A, 208, 213
Koch, R. H., Sobieski, S., & Wood, F. B. 1963, Pub. Univ. of Pennsylvania, Astro. Series 9
Kurtz, D. W., & Müller, M. 2001, MNRAS, 325, 1341
Malfait, K., Bogaert, E., & Waelkens, C. 1998, A&A, 331, 211
Mazzitelli, I. 1989, ApJ, 340, 249
Mazzitelli, I., D'Antona, F., & Caloi, V. 1995, A&A, 302, 382
Merin, B., Montesinos, B., Eiros, C., et al. 2004, A&A, 419, 301
Meeus, G., Waelkens, C., & Malfait, K. 1998, A&A, 329, 131
Mora, A., Natta, A., Eiroa, C., et al. 2002, A&A, 393, 259
Mora, A., Eiroa, C., Natta, A., et al. 2004, A&A, 419, 225
Muzerolle, J., D'Alessio, P., Calvet, N., & Hartmann, L. 2004, ApJ, 617, 406
Natta, A., Grinin, V. P., & Tambovtseva, L. V. 2000, ApJ, 542, 421
Oudmaijer, R. D., Palacios, J., Eiroa, C., et al. 2001, A&A, 379, 564
Paatz, G., & Camenzind, M. 1996, A&A, 308, 77
Pérez, M. R., van den Ancker, M. E., de Winter, D., & Bopp, B. W. 2004, A&A, 416, 647
Perryman, M. A. C., Lindegren, L., Kovalevsky, J., et al. 1997, A&A, 323, 49
Racine, R. 1968, AJ, 73, 233
Shu, F., Najita, J., Ostriker, E., et al. 1994, ApJ, 429, 781
Slawson, R. W., Hill, R. J., & Landstreet, J. D. 1992, ApJ, 82, 117
Thé, P. S., de Winter, D., & Pérez, M. R. 1994, A&AS, 104, 315
Valenti, J. A., & Piskunov, N. 1996, A&AS, 118, 59 5
van den Ancker, M. E, Thé, P. S., Tjin A Djie, H. R. E., et al. 1997, A&A, 324, L33
van der Veen, W. E. C. J., Waters, L. B. F. M., Trams, N. R., & Matthews, H. E. 1994, A&A, 285, 551
Ventura, P., Zeppieri, A., Mazzitelli, I., & D'Antona, F. 1998, A&A, 334, 953
Vieira, S. L. A., Pogodin, M. A., & Franco, G. A. P. 1999, A&A, 345, 559
Vieira, S. L. A., Corradi, W. J. B., Alencar, S. H. P., et al. 2003, AJ, 126, 2971
Wade, G. A., Drouin, D., Bagnulo, S., et al. 2005, A&A, 442, 31
Wolf, G. W., & Kern, J. T. 1983, ApJ, 52, 429